

# Accepted Manuscript

Natural History Study of Retinal Structure, Progression and Symmetry Using Ellipsoid Zone Metrics in *RPGR*-Associated Retinopathy

James J.L. Tee, Yesa Yang, Angelos Kalitzeos, Andrew Webster, James Bainbridge, Michel Michaelides



PII: S0002-9394(18)30584-1

DOI: [10.1016/j.ajo.2018.10.003](https://doi.org/10.1016/j.ajo.2018.10.003)

Reference: AJOPHT 10716

To appear in: *American Journal of Ophthalmology*

Received Date: 24 April 2018

Revised Date: 30 September 2018

Accepted Date: 1 October 2018

Please cite this article as: Tee JLL, Yang Y, Kalitzeos A, Webster A, Bainbridge J, Michaelides M, Natural History Study of Retinal Structure, Progression and Symmetry Using Ellipsoid Zone Metrics in *RPGR*-Associated Retinopathy, *American Journal of Ophthalmology* (2018), doi: <https://doi.org/10.1016/j.ajo.2018.10.003>.

This is a PDF file of an unedited manuscript that has been accepted for publication. As a service to our customers we are providing this early version of the manuscript. The manuscript will undergo copyediting, typesetting, and review of the resulting proof before it is published in its final form. Please note that during the production process errors may be discovered which could affect the content, and all legal disclaimers that apply to the journal pertain.

**Abstract**

**Purpose:** Quantitative study of retinal structure, progression rates and interocular symmetry in *RPGR*-associated retinopathy using spectral domain optical coherence tomography (SD-OCT).

**Design:** Prospective, observational cohort study.

**Methods:**

**Setting:** Moorfields Eye Hospital, London, UK

**Subjects:** 38 subjects

**Main outcome measure:** Two SD-OCT-derived ellipsoid zone (EZ) metrics with repeatability assessments. EZ width (EZW) measurements were made on transfoveal line scans. *En face* images of the EZ area (EZA) were generated from high density macular volume scans and quantified. Baseline size, progression rate, symmetry, associations with age and genotype, and baseline structure-function correlation were investigated.

**Results:** Baseline EZW and EZA were 1963.6  $\mu\text{m}$  and 3.70  $\text{mm}^2$  respectively. Mean EZW progression rate was 233.6  $\mu\text{m}/\text{year}$  and mean EZA rate was 0.67  $\text{mm}^2/\text{year}$ . Relative Interocular Difference as an index of symmetry was 3% for both metrics indicating good baseline symmetry in general although significant variation existed across the cohort. ANOVA results demonstrated a significant effect of age but not genotype on EZ dimension and progression rates. Larger EZ dimension and greater progression were seen in younger subjects. A positive correlation between EZ dimension and progression was evident. Overall exponential decline rates of 8.2% with EZW and 15.5% with EZA were obtained. Good functional correlation was found with EZW demonstrating stronger correlation, however EZA correlation with function was also significant.

**Conclusions:** EZ metrics are sensitive structural biomarkers for measuring residual extent and progression in *RPGR*-associated retinopathy. Our elucidation of the natural history will provide clinicians and patients with more knowledge about the condition, and inform the design and interpretation of interventional trials.

**Title: Natural History Study of Retinal Structure, Progression and Symmetry Using Ellipsoid Zone Metrics in *RPGR*-Associated Retinopathy**

**Authors:**

James J.L. Tee,<sup>1,2</sup> Yesa Yang,<sup>1,2</sup> Angelos Kalitzeos,<sup>1,2</sup> Andrew Webster,<sup>1,2</sup> James Bainbridge,<sup>1,2</sup> Michel Michaelides,<sup>1,2</sup>

1. UCL Institute of Ophthalmology, University College London, 11-43 Bath Street, London, EC1V 9EL, UK.
2. Moorfields Eye Hospital, City Road, London, EC1V 2PD, UK.

**Corresponding Author:** Michel Michaelides, UCL Institute of Ophthalmology, 11-43 Bath Street, London, EC1V 9EL, UK. E-mail: [michel.michaelides@ucl.ac.uk](mailto:michel.michaelides@ucl.ac.uk) Tel.no. +44 207 608 6864.

## **Introduction**

Retinitis pigmentosa (RP) secondary to sequence variants in the retinitis pigmentosa GTPase regulator gene (*RPGR*) constitute around three-quarters of all X-linked (XL) RP<sup>1-4</sup>, with *RP2* variants predominantly accounting for the remaining cases<sup>1,3,5-7</sup>. There is particular interest in *RPGR*-associated RP with recently commenced gene therapy trials currently underway (NCT03116113, NCT03252847 and NCT03316560).

Spectral-domain optical coherence tomography (SD-OCT) is in widespread use as an imaging modality to study retinal structure in a myriad of diseases. Previous OCT studies in RP have reported structural changes occurring at the transition zone as the scanned region of interest traverses from healthy central retinal tissue to diseased periphery<sup>8,9</sup>. Structural measurements of ellipsoid zone (EZ) width in RP, as a metric of disease severity and progression, have been shown to correlate well with retinal function<sup>10-13</sup>. Serial measurements of EZ width (EZW) to assess progression in XLRP have been studied<sup>14-17</sup>; however, these studies were potentially limited by bias in eye selection<sup>14-16</sup>, do not distinguish between genetic causes of XLRP<sup>14,15</sup>, or are retrospective<sup>17</sup>. The quantification of ellipsoid zone area (EZA), made possible with the use of vendor software to construct *en face* images from SD-OCT volume scans, has been demonstrated to be feasible in quantifying progression in autosomal recessive (AR) RP<sup>18</sup>. Despite this there has not been further studies on the use of EZA as a structural metric in RP.

We have therefore investigated the following in this protocol-driven prospective SD-OCT study comprising solely of RP subjects with molecularly confirmed pathogenic *RPGR* mutations: (i) intra-observer repeatability with EZW and EZA metrics; (ii) characterize baseline retinal structure with both metrics; (iii) characterize progression with both metrics; (iv) characterize interocular symmetry at baseline and progression and establish indices to quantify symmetry with both metrics; (v) investigate correlations between baseline measurements, progression and age; (vi) investigate effects of age and genotype on baseline and progression; (vii) determine overall exponential rates of progression with both metrics; and (viii) investigate structure-function correlations at baseline with both EZW and EZA metrics.

## **Methods**

Approval was granted by the ethics committee at Moorfields Eye Hospital prior to conducting the study. The declaration of Helsinki was adhered to throughout. All subjects were affected males with RP secondary to molecularly confirmed disease-causing mutations in *RPGR*. Bidirectional sequencing to test for mutations in *RPGR* exons 1-14 and Open Reading Frame 15 (ORF15) was performed at the Central Manchester University Hospitals Genomic Diagnostics Laboratory, UK, prior to recruitment.

### **OCT Acquisition and Analysis**

Dedicated clinical research ophthalmic technicians acquired protocol-driven OCT scans from both eyes of each subject at each visit, with the Spectralis OCT device (Heidelberg Engineering, Heidelberg, Germany). Horizontal high-resolution transfoveal line scans were

obtained using automated real-time tracking (ART) with an average of 100 images. Automatic registration was used for all follow-up scans to ensure accurate correspondence of retinal locations. Following line scan acquisition, bilateral macular high-resolution volume scans were acquired at the same visit. Each volume scan comprised of 193 horizontal b-scans in high resolution mode with 30  $\mu\text{m}$  distance between b-scans. Volume scans were purposefully acquired to allow the creation of *en face* images of the ellipsoid zone area (EZA). Following a departmental upgrade to the Spectralis OCT imaging platform with OCT2 module (Heidelberg Engineering, Heidelberg, Germany), volume scans acquired after June 2016 were captured with an average of 12 images (ART12) per horizontal b-scan, as allowed for by increased hardware capabilities and faster scanning speed with significant reduction in acquisition time.

Image analyses for both EZW and EZA metrics were performed using vendor software (Heidelberg Eye Explorer Version 1.10.2.0). EZW analyses were conducted on transfoveal line scan images with the following methodology: Images were displayed in a 1:1  $\mu\text{m}$  setting. The nasal and temporal extents of the EZ (point of EZ disappearance into the proximal RPE border with loss of outer segment layer) were identified and marked with the arrow tool. EZW was measured with the caliper tool as a straight line tangential to the distal RPE border (Figure 1). Line scan images were analyzed in a random order for each subject.

*En face* images of the EZA were created from each macular volume scan with the following method using vendor software: Images were created in a 3-dimensional mode and displayed in transverse view. The auto-segmented Bruch's membrane line was manually inspected for accurate placement along the outer border of the retinal pigment epithelium-Bruch's membrane complex as this line was utilized as a reference for the slab contour. The reference line was displaced a distance of 25  $\mu\text{m}$  inwards from Bruch's membrane and a slab of 30  $\mu\text{m}$  thickness was created. Slab settings were designed to capture the whole extent of the EZ layer in subjects. Following image creation, the EZA was delineated and measured using minimum intensity projection with area value provided by the vendor software (Figure 2).

### Statistics

For the assessment of intra-observer repeatability, EZW and EZA baseline images of each eye were measured twice by a single observer, a minimum of one week apart. Intra-observer repeatability assessment was also conducted on EZA derived from ART12 images (hereon referred to as EZA-ART12) acquired following upgrade to OCT2. One image per eye per subject was used to maintain the "independence-of-score" and to avoid inducing systematic bias. The method popularized by Bland and Altman was used to calculate mean  $\pm$  standard deviation (SD) of test-retest differences and corresponding 95% limits of agreement (LOA). Residuals were inspected for normality. Repeatability coefficient ( $RC = 1.96 * SD$ ) and the test-retest variability for both metrics were calculated and these are shown in Table 1.

The Bland Altman method was further utilized to assess interocular symmetry at baseline and progression as observed with both metrics (Table 2). An example is provided in Figure 3. Baseline EZW and EZA, EZW % rate and EZA % rate residuals were inspected for normality. Mean  $\pm$  SD of interocular difference, together with 95% LOA were calculated. Interocular

differences were obtained from the subtraction of left from right eyes. Mean of interocular differences was expressed as a fraction of its corresponding cohort average [cohort average in turn was calculated by obtaining the average of all interocular (mean of right and left eye) values of subjects] and this was presented as the Relative Interocular Difference (RID). The interocular coefficient (IC =  $1.96 * SD$ ), expressed as a fraction of the corresponding cohort average was calculated and presented as the Relative Interocular Variability (RIV). These indices were calculated to facilitate metric cross-comparison.

Progression rates for individual subjects were calculated by the following method: For each eye of each subject, ellipsoid zone measurements obtained with each metric were plotted as a function of age on separate scatterplots. As shown in Figure 4, linear trendlines were fitted to data points using a least squares method in Microsoft Excel (Mac version 15.41). Progression rates for each eye of each subject were obtained from trend line gradients.

Further statistical analyses were performed with XLSTAT version 2018.1 (Addinsoft, New York, NY). Data were inspected for normality and log transformation performed prior to conducting tests of statistical analyses where required. Interocular correlations at baseline and progression were investigated with the Pearson's correlation coefficient (Table 3). Following this, right and left eye data were combined to investigation correlation between age and baseline values, age and progression, and correlation between progression and baseline values (Table 3).

The effects of age and mutation on baseline and progression were assessed with a two-way analysis of variance (ANOVA) as shown in Table 4. Subject age was calculated from birth to time at baseline visit and was further divided into five categories: Category 1: <10 years of age, Category 2: 10 to <15 years, Category 3: 15 to <20 years, Category 4: 20 to <25 years, Category 5: 25 years of age and above. For the assessment of genotype, subjects were categorized into groups based on predicted effects of mutations: those will null allele mutations (premature stop codons or frameshifts leading to premature stop codons in exons 1-14) or those with mutations likely to result in translation of a variant protein product (missense mutations and mutations in ORF15). Splice site mutations were separately grouped owing to the unpredictability of their effects<sup>19</sup>. In instances of a significant ANOVA result, post-hoc multiple pairwise comparisons were conducted with Tukey's test.

Overall rates of progression for both metrics were modelled using a mixed-models method (Table 5). Analysis was performed with age (calculated from birth to time of OCT image acquisition) designated as a fixed effects quantitative explanatory variable. Each eye of each subject was designated as a random effects variable. Metric values were designated as dependent variables. Values were converted into natural log form to model an exponential decline. Previous studies have shown progression to be well characterized with an exponential decay model<sup>20-22</sup>, and this is further supported by evidence of exponential photoreceptor degeneration in animal models<sup>23</sup> and by inspection of our data (Figure 5). Distribution of model residuals were inspected for normality.

The association between structure and function was investigated. EZW and EZA data as a representation of baseline structure were correlated with data obtained from tests of visual

function performed at the same visit where available. Assessments of best corrected visual acuity (BCVA) were conducted with the Early Treatment Diabetic Retinopathy Study chart and contrast sensitivity (CS) assessments with the Pelli-Robson chart. BCVA was recorded in logarithm of the minimum angle of resolution (logMAR) units and CS as logCS units. Automated static perimetry testing was performed on the Octopus 900 (Haag-Streit AG, Köniz, Switzerland) using a customized, radially oriented 185-point grid. Perimetry mean sensitivity (MS) values in decibel units were obtained from vendor software. The volumetric measures of  $V_{\text{Total}}$  and  $V_{30}$  in decibel-steradian units were obtained following analysis of perimetry data with a third party software (Visual Field Modeling and Analysis software). In essence, both  $V_{\text{Total}}$  and  $V_{30}$  are metrics that characterize the total amount of sensitivity in the hill-of-vision as defined by the entire test grid ( $V_{\text{Total}}$ ) or that which is contained within a central circle of  $30^\circ$  radius ( $V_{30}$ ). A comprehensive description can be found in a recent publication<sup>24</sup>.

Significance level alpha for all statistical tests was set at 0.025 following Bonferroni correction for simultaneous analysis on two metrics (EZW and EZA).

## **Results**

All thirty-eight subjects in this study possessed bilateral ellipsoid zones visible at time of baseline imaging. Mean  $\pm$  SD age for all subjects at baseline was  $19.41 \pm 8.32$  years, ranging from 8.37 to 42.12 years. Seventeen subjects possessed mutations in Exon 1-14 and 21 in ORF15. Ten were predicted null allele mutations (all harboring Exon1-14 mutations), 25 predicted variant protein product (of which 4 were Exon 1-14 mutations, and 21 ORF15 mutations) and 3 splice site mutations. Bilateral macular OCT volume scans for *en face* analysis were successfully acquired at baseline for a subset of 31 subjects. Mean  $\pm$  SD age for 31 subjects was  $20.79 \pm 8.47$ , ranging from 8.37 to 42.12 years.

### **Progression Analysis**

For the calculation of progression rates, linear trend lines were plotted for subjects with OCT follow-up spanning a period greater than one year's duration, with a minimum of three imaging visits. 28 subjects had bilateral rates calculated with EZW metric. Mean  $\pm$  SD follow-up interval for these 28 subjects was  $2.05 \pm 0.72$  years, ranging from 1.10 to 3.81 years. 21 subjects had bilateral rates calculated with EZA metric. Mean  $\pm$  SD follow-up interval for these 21 subjects was  $2.00 \pm 0.74$  years, ranging from 1.01 to 3.51 years.

### **Test-retest Repeatability Analysis**

A comprehensive analysis of intra-observer test-retest repeatability is presented in Table 1. For both metrics, the mean of test-retest differences was small in comparison with baseline values. For EZW metric, mean test-retest difference was  $21.3 \mu\text{m}$  in comparison to mean EZW baseline of  $1963.6 \mu\text{m}$ . Likewise, for EZA metric, mean test-retest difference was  $0.025 \text{ mm}^2$  in comparison to mean baseline value of  $3.70 \text{ mm}^2$ . Calculated 95% LOA lay between  $-315.7 \mu\text{m}$  to  $273.1 \mu\text{m}$  for EZW, between  $-1.06 \text{ mm}^2$  to  $1.01 \text{ mm}^2$  for EZA, and between  $0.73$  to  $0.57 \text{ mm}^2$  for EZA-ART12. Test-retest variability of 15% for EZW was comparable to test-retest variability of 17% for EZA-ART12, in comparison to a test-retest variability of 28% for EZA.

### Baseline Values, Progression rates and Assessment of Interocular Symmetry

Descriptive statistics for baseline values and progression rates are provided in Table 2, together with indices of interocular symmetry. One subject (Figure 1) was excluded from symmetry analysis as the discrepancy between right and left eye was very large and resulted in an outlier effect and not at all in keeping with the entire cohort. Differences in mean EZW values at baseline for right eyes (1923.8  $\mu\text{m}$ ) and left eyes (2003.4  $\mu\text{m}$ ) were statistically insignificant ( $p=0.6750$ , paired samples  $t$ - test). Differences in mean EZA values at baseline for right eyes (3.37  $\text{mm}^2$ ) and left eyes (4.01  $\text{mm}^2$ ) were also statistically insignificant ( $p=0.8177$ , paired samples  $t$ - test).

Interocular differences in progression rates were statistically insignificant as assessed with both metrics. Mean EZW rate was 236.82  $\mu\text{m}/\text{year}$  for right eyes and 230.28  $\mu\text{m}/\text{year}$  for left eyes ( $p = 0.9479$ , paired samples  $t$ - test). Mean EZA rate was 0.61  $\text{mm}^2/\text{year}$  for right eyes and 0.73  $\text{mm}^2/\text{year}$  for left eyes ( $p = 0.3346$ , paired samples  $t$ - test). Equivalent annual progression rates in percentage for EZW was 13.6% for right eyes and 12.8% for left eyes. Equivalent annual progression rates in percentage for EZA was 16.0% for right eyes and 17.5% for left eyes.

A very strong interocular correlation at baseline was seen with both EZW and EZA metrics ( $r \geq 0.94$ ,  $p < 0.0001$ ), and for EZA-derived progression ( $r = 0.93$ ,  $p < 0.0001$ ) as shown in Table 3. Interocular correlation for EZW-derived progression was also strong ( $r = 0.65$ ,  $p = 0.0002$ ), albeit of a lesser magnitude in comparison to EZA-derived rates.

Further analysis of interocular symmetry was performed with the Bland-Altman method. Results are given in Table 2. A good level of interocular symmetry is evident with the use of both metrics to characterize baseline structure. This is reflected in RID values of 3.34% and 3.07% for EZW and EZA respectively. The RIV, as an index of variability in interocular symmetry at baseline, was larger with EZW metrics at 31.87% compared with an RIV of 17.58% when baseline structure was characterized by the EZA metric.

A greater level of symmetry was seen with the use of EZW over EZA metric when characterizing progression. RID for EZW rates was 1.54% compared to 8.93% for EZA. There was however greater variability with the use of EZW over EZA. RIV was 102.60% for rates defined with EZW compared with 78.01% for rates defined with EZA metric.

### Associations of Age, Baseline and Progression

Correlation data are shown in Table 3. All correlations were statistically significant. A strong negative association between age and baseline is evident with both metrics ( $r = -0.61$ ,  $p < 0.0001$  for EZW;  $r = -0.64$ ,  $p < 0.0001$  for EZA). A moderate to strong negative correlation was seen between age and progression ( $r = -0.58$ ,  $p < 0.0001$  for EZW;  $r = -0.74$ ,  $p < 0.0001$  for EZA). A strong positive correlation between baseline and progression was evident with EZA ( $r = 0.83$ ,  $p < 0.0001$ ), with a weaker positive correlation seen with EZW metric ( $r = 0.45$ ,  $p = 0.0005$ ).

The effects of age and mutation on baseline values and progression rates were further interrogated with a two-way ANOVA. Results together with mean  $\pm$  SD values for each



category are shown in Table 4. The effect of age was significant on baseline and progression rates as determined by both EZW and EZA metrics. Post-hoc pairwise comparisons revealed significant differences between subjects in age categories 1 and 2 versus age categories 4 and 5. In contrast, the effects of mutation on baseline and progression rates were insignificant.

### **Mixed-Models Analyses to Determine Overall Progression**

Overall rates of progression for the entire cohort was modelled using EZW and EZA data. As shown in Table 5, an annual exponential decline rate of 8.22% was obtained with EZW data. A greater exponential rate of 15.47% for the cohort was obtained with EZA data.

### **Associations of Structure and Function**

Correlations between structure and function at baseline are shown in Table 6. All correlations were statistically significant. EZW correlated strongly with functional metrics  $V_{\text{Total}}$ , CS and MS ( $r = 0.64, 0.64$  and  $0.63$  respectively). The same functional metrics ( $V_{\text{Total}}$ , CS and MS) also showed greatest correlations with EZA ( $r = 0.48, 0.60$  and  $0.45$  respectively). Correlations between EZW with  $V_{30}$  and BCVA were moderate in strength ( $r = 0.59$  and  $-0.40$  respectively). Correlations between EZA with  $V_{30}$  and BCVA were weaker, albeit still significant ( $r = 0.38$  and  $-0.37$  respectively).

### **Discussion**

Herein we describe the first protocol-driven SD-OCT study to characterize EZ changes in subjects with molecularly proven *RPGR*-associated RP, using both *en face* generated EZA and transfoveal EZW metrics.

Mean of individual progression rates in our cohort, as calculated by linear trend lines for each eye, was  $234 \mu\text{m}/\text{year}$  with the EZW metric. This is comparable, albeit slightly less than mean progression rates in XLRP reported by others utilizing a similar metric:  $248 \mu\text{m}/\text{year}$ <sup>14</sup>,  $270 \mu\text{m}/\text{year}$ <sup>15</sup>, and  $289 \mu\text{m}/\text{year}$ <sup>16</sup>. Note however that subjects for these three studies were obtained from the same source, i.e. the DHA trial (NCT00100230)<sup>25</sup> and thus there is likely to be a degree of subject overlap in the three studies. Our equivalent mean annual progression rate is 13.2% relative to baseline values. This is greater than the annual rate of 9.6% previously reported in a study with mean baseline EZW of  $3410 \mu\text{m}$ <sup>16</sup>. On average, subjects in our cohort possessed a smaller residual baseline EZ.

With the EZA metric, the mean of individual progression rates in our cohort, as calculated by linear trendlines for each eye, was  $0.67 \text{ mm}^2/\text{year}$  (16.7%/year). This is comparable to a previously reported progression rate of  $0.64 \text{ mm}^2/\text{year}$  (percentage rate equivalent was not provided)<sup>15</sup> in a study where the EZA analysis was performed via layer segmentation and the use of third party software as acquired volume scans of 31 b-scan density were not sufficiently dense to permit the construction of *en face* images with vendor software.

To our knowledge, the use of *en face* images to quantify EZA changes in RP has been carried out by just one other study, albeit on subjects with ARRP<sup>18</sup>. A mean progression rate of 0.27

mm<sup>2</sup>/year (13%/year) was reported, however subjects were followed for only one year and progression rate calculated from images acquired at just two-time points<sup>18</sup>.

The other studies on XLRP described above have also calculated progression with data from only two time points, taken an average of two years apart.<sup>15,16</sup> In these studies, only one eye of each subject was chosen for analysis; and in the presence of multiple scans, the one with the clearest EZ band was chosen<sup>16</sup>. Thus, the possibility of selection bias influencing results of these studies cannot be excluded.

We have taken a different and arguably more robust approach in our study. Data were acquired from both eyes and analyzed separately and then together. Images from multiple time points (a minimum of three time points) were analyzed to plot individual trend lines, from which progression rates were obtained from the slopes of trend lines. A similar approach to calculating progression rates from slopes of linear trend lines has been used by Sujirakul and Cabral<sup>26,27</sup> in their analyses of EZW, with reported mean progression rate of 140 µm/year (5.2%/year). Their cohort however comprised RP subjects with various inheritances (of which only 5% had XLRP) and thus rates are not directly comparable.

We were able to plot an exponential decline using a mixed-models approach, with data taken collectively which afforded a wide age span. Here we found a progression rate of 8.22% per year with the EZW metric, and 15.47% per year with the EZA metric. Our EZA rate, which is roughly twice the EZW progression rate, fulfils the mathematical prediction of a doubling of rate with progression tracked by area metrics. [Area of a circle =  $\pi (d/2)^2$ ]. With the simultaneous use of both EZW and EZA metrics we are thus able to prove this hypothesis which has been previously alluded to<sup>14,16</sup>.

Arguably the exponential rates calculated may, in general, be more reflective of the average decline present in the population. Nonetheless phenotypic heterogeneity is evident in this condition as demonstrated by our subjects, necessitating individual observations to be made.

### **Interocular Symmetry**

There is a good level of interocular symmetry at baseline, with an RID of 3% for both EZW and EZA metrics. When characterizing progression, greater interocular symmetry was found with the use of EZW over the use of EZA metrics. RID for EZW rates was 1.54% compared to 8.93% for EZA rates.

Nevertheless, there was significant variation in the degree of interocular symmetry seen across the cohort, as typified by the RIV. RIV at baseline was 17.6% and 31.9% respectively for EZA and EZW metrics. RIV for progression rates were 78.0 % and 102.6% for EZA and EZW respectively.

Despite this level of variation described, interocular correlation at baseline as assessed with both metrics were very strong ( $r \geq 0.94$ ,  $p < 0.0001$ ). Interocular correlation for progression as characterized by EZA ( $r = 0.93$ ,  $p < 0.0001$ ) and EZW ( $r = 0.65$ ,  $p = 0.0002$ ) were also strong and significant. In addition, interocular differences at baseline and for progression rates with both metrics were statistically insignificant when tested with the paired samples t-test.

This highlights the inadequacies of using correlation analyses as a sole method for assessing interocular symmetry.

As an example, the mean baseline EZW in our cohort was 1964  $\mu\text{m}$ . Despite a small mean interocular difference of 64  $\mu\text{m}$ , the 95% LOA reached 669  $\mu\text{m}$ . Thus, the implication is that observations are necessary for all subjects before inferring the presence of good interocular symmetry. As such, one can argue that in-depth natural history studies are a requirement prior to treatment trials for many reasons, including this.

### **Test-retest Variability**

The 15% test-retest variability for EZW is comparable, albeit marginally smaller than the 17% test-retest variability found with EZA-ART12. In comparison, test-retest variability was 28% for EZA measurements derived from volume scans acquired without averaging. This finding indicates that both EZW and EZA-ART12 measurements are metrics with similar precision. Test-retest variability for both EZW and EZA-ART12 are equivalent to corresponding annual progression rates of 13% and 17% respectively.

The greater precision seen with EZW and EZA-ART12 measurements is not unexpected. EZW measurements were made on transfoveal line scans acquired with an average of 100 images each, thus rendering a high signal to noise ratio. This high average number of images is achievable as only one line scan is obtained per transfoveal image.

Following procurement of the Spectralis OCT2 module (Heidelberg Engineering), the significant reduction in acquisition time allowed high-resolution volume scans to be obtained with an average of 12 images per b-scan while maintaining the 193 b-scan density of each scan. EZA borders were more clearly visible on *en face* images generated from these ART12 volume scans (Figure 2), thus allowing for greater precision and better measurement repeatability, in contrast to EZA measurements made on images generated from earlier volume scans acquired without averaging.

### **Test-retest Variability Reported in Other Studies**

None of the aforementioned studies assessed observer repeatability in XLRP subjects despite studying XLRP cohorts. One study selected 13 subjects with ADRP (from 59 subjects including 26 with XLRP) with images measured twice over an unspecified time interval. Their intra-observer test-retest variability was estimated at 7.3% with a repeatability coefficient of 0.9 degrees (260  $\mu\text{m}$ ) and mean baseline EZW of 12.4 degrees (3584  $\mu\text{m}$ ). Mean annual constriction rate for their adRP cohort was 3.4%, indicating their test-retest variability was twice the annual constriction rate for the tested subjects<sup>16</sup>.

Two related studies<sup>14,15</sup> assessed repeatability in image acquisition but not image measurement. In both studies, a different group of RP patients (AR or simplex RP) to those reported were imaged twice on the same day. Another study whose cohort comprised of RP of mixed inheritances assessed intra-observer repeatability with images measured twice several weeks apart, and reported a repeatability coefficient of 233  $\mu\text{m}$  with test-retest variability of 8.9%, which is almost twice that of their cohort annual constriction rate of 4.9%<sup>26</sup>.

### Comparisons of Test-retest Variability with Indices of Interocular Symmetry

The mean of intra-observer test-retest difference is small in comparison to the mean of interocular difference for both metrics. For EZW, mean of intra-observer test-retest difference is 21.3  $\mu\text{m}$  compared to 63.5  $\mu\text{m}$  for mean of interocular difference. For EZA metric, mean intra-observer test-retest difference is 0.03  $\text{mm}^2$ , in comparison to 0.10  $\text{mm}^2$  for mean of interocular difference. Thus, both metrics are suitable for use as structural OCT measures to quantify disease.

The 95% LOA for interocular symmetry with the EZW metric was -542  $\mu\text{m}$  to 669  $\mu\text{m}$ . In comparison, corresponding 95% LOA for test-retest repeatability was -316  $\mu\text{m}$  to 273  $\mu\text{m}$ . Likewise, test-retest repeatability coefficient of 294  $\mu\text{m}$  for EZW is less than half its corresponding interocular coefficient of 605  $\mu\text{m}$ . This finding of a test-retest repeatability that is under half that of expected interocular symmetry values further indicates that the EZW metric is reliable for use, especially where quantification of disease in the fellow eye is important, for example in cases where the fellow eye would be expected to act as a control to the eye undergoing the treatment trial.

With regards to the EZA metric, the 95% LOA for interocular symmetry of -0.49  $\text{mm}^2$  to 0.70  $\text{mm}^2$ , is approximately similar to the corresponding 95% LOA for test-retest repeatability of -0.73  $\text{mm}^2$  to 0.57  $\text{mm}^2$  obtained with EZA-ART12. Test-retest repeatability coefficient of 0.65  $\text{mm}^2$  is also approximately similar to the corresponding interocular coefficient of 0.59  $\text{mm}^2$ . These findings again indicate that the EZA is a suitable metric for use particularly when measurements are derived from dense volume scans obtained with good image averaging protocols.

The 95% LOA for EZA test-retest repeatability performed on scans acquired without averaging was larger at -1.06  $\text{mm}^2$  to 1.01  $\text{mm}^2$ . As mentioned, EZA measurements were not as precise when made on *en face* images derived from volume scans acquired without averaging on the OCT1 during the initial period of the study. Nevertheless, these earlier EZA findings are of value and can play an important role as a secondary OCT metric to corroborate and confirm findings made with the EZW metric.

### Associations and Effects of Age on Baseline and Progression Rates

We found a strong negative correlation between age and baseline, indicating that the EZ is smaller in older eyes. The moderate to strong negative correlation found between age and progression rates, together with the strong positive correlation between baseline and progression indicates that in general, progression is greater in younger eyes possessing a larger baseline.

Results from the ANOVA (Table 4) further demonstrate the significant effects of age on baseline and progression rates. The largest baseline values and progression rates are seen in the youngest subjects of the cohort. Post-hoc comparisons confirm the biggest differences in baseline and rates were between subjects in younger age categories (Categories 1 and 2) compared to those in the older age categories (Categories 4 and 5). In contrast, the effects of mutation on baseline and progression were insignificant. Our current findings substantiate those of our previous work<sup>17,22</sup>.

### **Correlation of Structure and Function**

We have demonstrated good functional correlation with the use of both EZW and EZA as structural metrics. Correlations between EZW and functional metrics were stronger overall, however functional correlations with EZA were also significant. These findings provide further support for the use of both structural metrics as surrogate markers of disease in *RPGR*-RP; with the demonstrated functional correlation being of key importance to both patients and regulators alike.

In conclusion, we have provided and discussed prospectively acquired SD-OCT data in a cohort of subjects with *RPGR*-RP with a particular focus on the EZ as a structural biomarker of disease. The use of two distinct EZ metrics together in conjunction adds to the robustness of this study. Both EZW and EZA metrics provide sensitive and complementary parameters to characterize structure and progression in the condition. We anticipate our natural history findings to inform recently commenced *RPGR* treatment trials, both in the recruitment of trial subjects as well as in adjudicating treatment response. Our findings will also be of use to clinicians caring for patients with *RPGR*-RP and other researchers in the expanding field of phenotyping inherited retinal conditions.

### **Funding/Support**

Supported by grants from the National Institute for Health Research Biomedical Research Centre at Moorfields Eye Hospital National Health Service Foundation Trust and UCL Institute of Ophthalmology (UK), Fight For Sight (UK), MeiraGTx, Moorfields Eye Hospital Special Trustees (UK), Moorfields Eye Charity (UK), the Foundation Fighting Blindness (USA), Retinitis Pigmentosa Fighting Blindness (UK), and the Wellcome Trust [099173/Z/12/Z]. Michel Michaelides is supported by an FFB Career Development Award.

**Financial Disclosures:** Michel Michaelides and James Bainbridge consult for and are shareholders in MeiraGTx.

### **References**

1. Sharon D, Sandberg MA, Rabe VW, Stillberger M, Dryja TP, Berson EL. RP2 and RPGR mutations and clinical correlations in patients with X-linked retinitis pigmentosa. *Am J Hum Genet.* 2003;73(5):1131-1146.
2. Shu X, Black GC, Rice JM, et al. RPGR mutation analysis and disease: an update. *Human Mutat.* 2007;28(4):322-328.
3. Pelletier V, Jambou M, Delphin N, et al. Comprehensive survey of mutations in RP2 and RPGR in patients affected with distinct retinal dystrophies: genotype-phenotype correlations and impact on genetic counseling. *Human Mutat.* 2007;28(1):81-91.
4. Tee JJ, Smith AJ, Hardcastle AJ, Michaelides M. RPGR-associated retinopathy: clinical features, molecular genetics, animal models and therapeutic options. *Br J Ophthalmol.* 2016;100(8):1022-1027.

5. Schwahn U, Lenzner S, Dong J, et al. Positional cloning of the gene for X-linked retinitis pigmentosa 2. *Nat Genet.* 1998;19(4):327-332.
6. Hardcastle AJ, Thiselton DL, Van Maldergem L, et al. Mutations in the RP2 gene cause disease in 10% of families with familial X-linked retinitis pigmentosa assessed in this study. *Am J Hum Genet.* 1999;64(4):1210-1215.
7. Breuer DK, Yashar BM, Filippova E, et al. A comprehensive mutation analysis of RP2 and RPGR in a North American cohort of families with X-linked retinitis pigmentosa. *Am J Hum Genet.* 2002;70(6):1545-1554.
8. Jacobson SG, Aleman TS, Sumaroka A, et al. Disease boundaries in the retina of patients with Usher syndrome caused by MYO7A gene mutations. *Invest Ophthalmol Vis Sci.* 2009;50(4):1886-1894.
9. Hood DC, Lazow MA, Locke KG, Greenstein VC, Birch DG. The transition zone between healthy and diseased retina in patients with retinitis pigmentosa. *Invest Ophthalmol Vis Sci.* 2011;52(1):101-108.
10. Aizawa S, Mitamura Y, Baba T, Hagiwara A, Ogata K, Yamamoto S. Correlation between visual function and photoreceptor inner/outer segment junction in patients with retinitis pigmentosa. *Eye (Lond).* 2009;23(2):304-308.
11. Fischer MD, Fleischhauer JC, Gillies MC, Sutter FK, Helbig H, Barthelmes D. A new method to monitor visual field defects caused by photoreceptor degeneration by quantitative optical coherence tomography. *Invest Ophthalmol Vis Sci.* 2008;49(8):3617-3621.
12. Hood DC, Ramachandran R, Holopigian K, Lazow M, Birch DG, Greenstein VC. Method for deriving visual field boundaries from OCT scans of patients with retinitis pigmentosa. *Biomed Opt Express.* 2011;2(5):1106-1114.
13. Birch DG, Locke KG, Feliuss J, et al. Rates of decline in regions of the visual field defined by frequency-domain optical coherence tomography in patients with RPGR-mediated X-linked retinitis pigmentosa. *Ophthalmology.* 2015;122(4):833-839.
14. Birch DG, Locke KG, Wen Y, Locke KI, Hoffman DR, Hood DC. Spectral-domain optical coherence tomography measures of outer segment layer progression in patients with X-linked retinitis pigmentosa. *JAMA Ophthalmol.* 2013;131(9):1143-1150.
15. Ramachandran R, Zhou L, Locke KG, Birch DG, Hood DC. A comparison of methods for tracking progression in X-linked retinitis pigmentosa using frequency domain OCT. *Transl Vis Sci Technol.* 2013;2(7):5.
16. Cai CX, Locke KG, Ramachandran R, Birch DG, Hood DC. A comparison of progressive loss of the ellipsoid zone (EZ) band in autosomal dominant and X-linked retinitis pigmentosa. *Invest Ophthalmol Vis Sci.* 2014;55(11):7417-7422.
17. Tee JLL, Carroll J, Webster AR, Michaelides M. Quantitative analysis of retinal structure using spectral-domain optical coherence tomography in RPGR-associated retinopathy. *Am J Ophthalmol.* 2017;178:18-26.
18. Hariri AH, Zhang HY, Ho A, et al. Quantification of ellipsoid zone changes in retinitis pigmentosa using en face spectral domain-optical coherence tomography. *JAMA Ophthalmol.* 2016;134(6):628-635.
19. Fahim AT, Bowne SJ, Sullivan LS, et al. Allelic heterogeneity and genetic modifier loci contribute to clinical variation in males with X-linked retinitis pigmentosa due to RPGR mutations. *PLoS One.* 2011;6(8):e23021.
20. Massof RW, Dagnelie G, Benzscharow T. First order dynamics of visual field loss in retinitis pigmentosa. *Clin Vision Sci.* 1990;5:1-26.

21. Sandberg MA, Rosner B, Weigel-DiFranco C, Dryja TP, Berson EL. Disease course of patients with X-linked retinitis pigmentosa due to RPGR gene mutations. *Invest Ophthalmol Vis Sci.* 2007;48(3):1298-1304.
22. Tee JLL, Kalitzeos A, Webster AR, Peto T, Michaelides M. Quantitative analysis of hyperautofluorescent rings to characterize the natural history and progression in RPGR-associated retinopathy. *Retina.* 2017. doi:10.1097/IAE.0000000000001871. [Epub ahead of print].
23. Clarke G, Collins RA, Leavitt BR, et al. A one-hit model of cell death in inherited neuronal degenerations. *Nature.* 2000;406(6792):195-199.
24. Tee JLL, Yang Y, Kalitzeos A, et al. Characterization of visual function, interocular variability and progression using static perimetry-derived metrics in RPGR-associated retinopathy. *Invest Ophthalmol Vis Sci.* 2018;59(6):2422-2436.
25. Hoffman DR, Hughbanks-Wheaton DK, Pearson NS, et al. Four-year placebo-controlled trial of docosahexaenoic acid in X-linked retinitis pigmentosa (DHAX trial): a randomized clinical trial. *JAMA Ophthalmol.* 2014;132(7):866-873.
26. Sujirakul T, Lin MK, Duong J, Wei Y, Lopez-Pintado S, Tsang SH. Multimodal imaging of central retinal disease progression in a 2-year mean follow-up of retinitis pigmentosa. *Am J Ophthalmol.* 2015;160(4):786-798.
27. Cabral T, Sengillo JD, Duong JK, et al. Retrospective analysis of structural disease progression in retinitis pigmentosa utilizing multimodal imaging. *Sci Rep.* 2017;7(1):10347.

### **Figure Captions**

Figure 1 shows horizontal transfoveal spectral domain optical coherence tomography scans of both eyes of a subject with *RPGR*-associated retinopathy. Vertical arrows mark the extent of the ellipsoid zone (EZ) on the scans. Ellipsoid zone width (EZW) was 7163  $\mu\text{m}$  in the left eye (shown in top image) and 1534  $\mu\text{m}$  in the right eye (shown in bottom image). Note that the large interocular difference found in this subject is not in keeping with the cohort.

Figure 2 is a composite of four images. Top row images show *en face* images of the ellipsoid zone area (EZA) generated from high resolution macular volume scans of two subjects with *RPGR*-associated retinopathy. Bottom row images show delineation and quantification of respective EZAs from the same top row images. Images on the right column were generated from a macular volume scan acquired with an average of 12 images per b-scan.

Figure 3 shows a Bland Altman plot illustrating interocular differences in ellipsoid zone width (EZW) at baseline. Interocular difference for each individual is plotted on the y-axis against the mean EZW value of both eyes. (Horizontal long dash line refers to the mean of interocular differences; horizontal dotted lines denote 95% limits of agreement).

Figure 4 shows linear trend lines indicating progression, plotted from observations of ellipsoid zone width. Each line represents the right eye of a subject. Data from twenty-eight subjects who underwent three or more observations over an interval greater than one year are shown.

Figure 5 shows scatterplots of ellipsoid zone width and ellipsoid zone area respectively, both plotted against subjects' age. An exponential decline is evident for both. The reader is directed to Table 5 for further information on exponential decline rates calculated with the mixed-models method.

ACCEPTED MANUSCRIPT



Metric	EZW			EZA			EZA-ART12		
	Right Eyes	Left Eyes	Both Eyes	Right Eyes	Left Eyes	Both Eyes	Right Eyes	Left Eyes	Both Eyes
Mean $\pm$ SD of intra-observer difference ( $\mu\text{m}$ for EZW/ $\text{mm}^2$ for EZA)	-8.26 $\pm$ 121.55	34.32 $\pm$ 174.99	-21.29 $\pm$ 150.22	-0.062 $\pm$ 0.513	0.013 $\pm$ 0.551	-0.025 $\pm$ 0.529	-0.110 $\pm$ 0.228	-0.040 $\pm$ 0.404	-0.076 $\pm$ 0.326
95% LOA ( $\mu\text{m}$ for EZW/ $\text{mm}^2$ for EZA)	-246.49 to 229.97	-377.29 to 308.66	-315.72 to 273.14	-1.067 to 0.943	-1.067 to 1.093	-1.062 to 1.013	-0.561 to 0.341	-0.824 to 0.744	-0.727 to 0.567
Repeatability coefficient	238.24	342.98	294.43	1.005	1.080	1.037	0.4508	0.7840	0.6468
Test-retest variability (%)	12.38	17.12	14.99	29.82	26.93	28.03	13.38	19.55	17.48

Table 1 shows intra-observer repeatability analysis of EZW and EZA measurements. Test-retest measurements were performed a minimum of one week apart on 76 eyes of 38 subjects for the EZW metric; 62 eyes of 31 subjects for the EZA metric; and 53 eyes of 27 subjects for EZA-ART12. Repeatability coefficient = 1.96 (SD).

EZW= ellipsoid zone width; EZA= ellipsoid zone area; ART12 = automatic real-time tracking with average of 12 images per horizontal b-scan; SD = standard deviation; LOA= limits of agreement.

Metric	All Eyes		Right Eyes		Left Eyes		Indices of Interocular Symmetry				
	Mean (SD)	95% CI	Mean (SD)	95% CI	Mean (SD)	95% CI	Mean (SD) of Interocular Difference	95% LOA	RID (%)	Interocular Coefficient	RIV (%)
<b>EZW baseline (<math>\mu\text{m}</math>)</b>	1963.59 (1541.76)	1611.28 to 2315.90	1923.79 (1447.35)	1448.06 to 2399.52	2003.39 (1649.31)	1461.28 to 2545.51	63.51 (308.79)	-541.72 to 668.74	3.34	605.23	31.87
<b>EZA baseline (<math>\text{mm}^2</math>)</b>	3.70 (6.14)	2.13 to 5.25	3.37 (5.60)	1.31 to 5.42	4.01 (6.72)	1.55 to 6.48	0.10 (0.30)	-0.49 to 0.70	3.07	0.59	17.58
<b>EZW Rate (<math>\mu\text{m}/\text{yr}</math>)</b>	233.55 (189.13)	182.90 to 284.20	236.82 (192.20)	162.30 to 311.35	230.28 (189.49)	156.80 to 303.75					
<b>EZW Rate (%/yr)</b>	13.20 (14.85)	9.22 to 17.18	13.59 (15.54)	7.57 to 19.62	12.81 (14.41)	7.22 to 18.39	0.20 (6.94)	-13.39 to 13.8	1.54	13.60	102.60
<b>EZA Rate (<math>\mu\text{m}/\text{yr}</math>)</b>	0.67 (0.95)	0.38 to 0.97	0.61 (0.83)	0.24 to 0.99	0.73 (1.07)	0.24 to 1.21					
<b>EZA Rate (%/yr)</b>	16.70 (11.19)	13.22 to 20.19	15.96 (9.56)	11.61 to 20.31	17.45 (12.81)	11.62 to 23.28	-1.49 (6.65)	-14.52 to 11.54	8.93	13.03	78.01

Table above describes baseline values and progression rates for EZW and EZA, together with respective indices of interocular symmetry. The number of eyes in the cohort for characterization of baseline EZW were 76 eyes of 38 subjects; baseline EZA with 62 eyes of 31 subjects; EZW rate with 56 eyes of 28 subjects; EZA rate with 42 eyes of 21 subjects. Positive progression rates indicate constriction occurring over time.

(EZW= ellipsoid zone width; EZA= ellipsoid zone area; SD= standard deviation; LOA= limits of agreement; RID= relative interocular difference; RIV= relative interocular variability).

Parameters	Pearson's correlation coefficient, r	P-value
Interocular correlation at baseline		
-EZW	0.9410	<0.0001
-EZA	0.9725	<0.0001
Interocular correlation of progression rate		
-EZW	0.6535	0.0002
-EZA	0.9340	<0.0001
Age with baseline		
-EZW	-0.6061	<0.0001
-EZA	-0.6381	<0.0001
Age with progression rate		
-EZW	-0.5751	<0.0001
-EZA	-0.7386	<0.0001
Baseline value with progression rate		
-EZW	0.4524	0.0005
-EZA	0.8307	<0.0001

Table above shows associations at baseline, progression and with age. Significance level alpha was set at 0.025 following Bonferroni correction for simultaneous analysis with two metrics (EZW and EZA).

(EZW= ellipsoid zone width, EZA = ellipsoid zone area).

ACCEPTED MANUSCRIPT

	Baseline EZW ( $\mu\text{m}$ )  Mean $\pm$ SD (no. of eyes)	Baseline EZA ( $\text{mm}^2$ )  Mean $\pm$ SD (no. of eyes)	EZW Rate ( $\mu\text{m}/\text{year}$ )  Mean $\pm$ SD (no. of eyes)	EZA Rate ( $\text{mm}^2/\text{year}$ )  Mean $\pm$ SD (no. of eyes)
<b>Age Categories</b>				
Category 1	3870.83 $\pm$ 1373.53 (12)	13.15 $\pm$ 9.06 (8)	351.52 $\pm$ 189.32 (10)	1.78 $\pm$ 1.21 (8)
Category 2	2950.93 $\pm$ 1534.45 (14)	8.27 $\pm$ 7.74 (8)	331.65 $\pm$ 174.52 (10)	2.04 $\pm$ 0.27 (2)
Category 3	1906.29 $\pm$ 1369.78 (14)	3.12 $\pm$ 3.22 (10)	302.76 $\pm$ 247.86 (10)	0.93 $\pm$ 0.77 (8)
Category 4	1038.72 $\pm$ 578.26 (18)	0.89 $\pm$ 0.79 (18)	160.95 $\pm$ 98.33 (14)	0.12 $\pm$ 0.06 (12)
Category 5	893.61 $\pm$ 453.09 (18)	0.57 $\pm$ 0.39 (18)	80.52 $\pm$ 70.10 (12)	0.08 $\pm$ 0.10 (12)
P-value (ANOVA)	<0.0001	<0.0001	0.0038	0.0002
Tukey's test	Category 1 vs Categories 4,5 ( $p < 0.0001$ for all); Category 2 vs Categories 4,5 ( $p < 0.0001$ ); category 1 vs category 3 ( $p = 0.0003$ ).	Category 1 vs Categories 4,5 ( $p < 0.0001$ for all); Category 1 vs 3 ( $p = 0.0002$ ); Category 2 vs Category 4 ( $p =$ 0.0029); Category 2 vs Category 5 ( $p =$ 0.0017)	Category 1 vs Category 5 ( $p = 0.0007$ ); Category 1 vs Category 4 ( $p = 0.0224$ ); Category 2 vs Category 5 ( $p = 0.0019$ ); Category 3 vs Category 5 ( $p = 0.0074$ )	Category 1 vs Categories 4,5 ( $p < 0.0001$ ); Category 2 vs 4 ( $p = 0.0059$ ); Category 2 vs Category 5 ( $p =$ 0.0050)

<b>Mutation Function</b>				
Null function	1446.40 ± 775.13 (20)	1.33 ± 1.26 (18)	106.86 ± 85.83 (18)	0.17 ± 0.22 (16)
Variant protein product	2170.58 ± 1714.84 (50)	4.89 ± 7.42 (38)	287.76 ± 184.88 (34)	0.98 ± 1.12 (22)
Splice site	1962.67 ± 1747.96 (6)	3.19 ± 4.10 (6)	342.83 ± 304.20 (4)	0.98 ± 1.06 (4)
P-value (ANOVA)	0.2049	0.6451	0.0672	0.9313
<b>Age and Mutation Function interaction</b>				
P-value (ANOVA)	0.9030	0.6997	0.0271	0.9492

Table above shows the results of a 2-way ANOVA investigating the effects of age and mutation function on baseline values and progression rates, as characterized by EZW and EZA. Significance level alpha was set at 0.025 following Bonferroni correction. Post-hoc multiple pairwise comparisons between the age categories were performed using Tukey's test with those reaching statistical significance shown. (Age categories: 1 = <10 years of age, 2 = 10 to < 15 years, 3 = 15 to < 20 years, 4 = 20 to < 25 years, 5 = ≥ 25 years).

(EZW= ellipsoid zone width; EZA= ellipsoid zone area; ANOVA= analysis of variance; SD= standard deviation)

Metric	Slope (95% CI); p-value	Annual % Exponential Decline Rate (95% CI)	Half-life (95% CI) in years
EZW	-0.0857 (-0.1024 to -0.0691); p<0.0001	8.22 (6.67 to 9.73)	8.09 (6.77 to 10.04)
EZA	-0.1680 (-0.1974 to -0.1387); p<0.0001	15.47 (12.95 to 17.91)	4.12 (3.51 to 5.00)

Table above shows overall progression modelled from EZW and EZA data. Annual exponential decline rates together with half-lives were calculated from slope values obtained using the mixed-models method with age designated as a fixed effects variable. All values were converted into natural log form prior to analyses in order to model an exponential decline. Half-lives with 95% confidence intervals were calculated with the equation  $t_{1/2} = -\log_e(2)/k$ . The significance of age exerting an effect on the model is denoted by the corresponding p-values. Significance level alpha was set at 0.025.

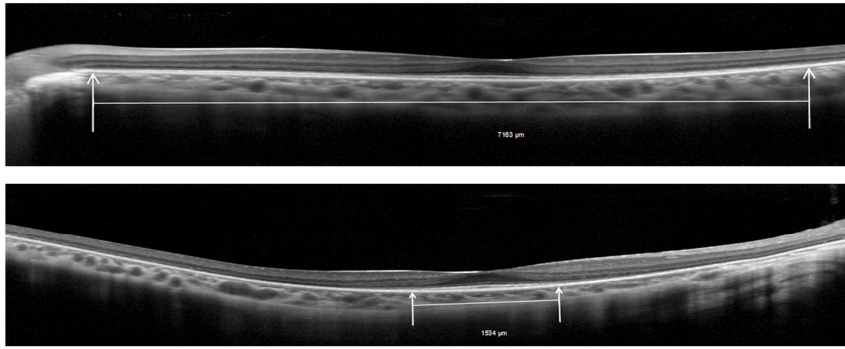
(EZW = ellipsoid zone width; EZA = ellipsoid zone area ; CI = confidence interval)

Parameter	EZW Pearson's correlation coefficient, r (P-value)	EZA Pearson's correlation coefficient, r (P-value)
BCVA	-0.3959 (0.0004)	-0.3741 (0.0027)
CS	0.6365 (<0.0001)	0.5967 (<0.0001)
MS	0.6279 (<0.0001)	0.4508 (0.0021)
$V_{Total}$	0.6372 (<0.0001)	0.4765 (0.0011)
$V_{30}$	0.5942 (<0.0001)	0.3791 (0.0112)

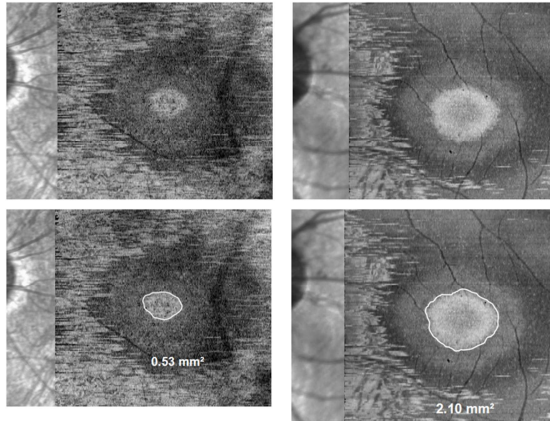
Table 6 above shows associations of structure and function at baseline. Significance level alpha was set at 0.025 following Bonferroni correction for simultaneous analysis with two structural metrics, EZW and EZA. Associations between EZW and BCVA/CS were studied on 76 eyes of 38 subjects. Associations between EZW and MS/ $V_{Total}$ / $V_{30}$  were studied on 53 eyes of 28 subjects (28 right and 25 left eyes). Associations between EZA and BCVA/CS were studied on 62 eyes of 31 subjects. Associations between EZA and MS/ $V_{Total}$ / $V_{30}$  were studied on 44 eyes of 23 subjects (23 right and 21 left eyes).

EZW = ellipsoid zone width, EZA = ellipsoid zone area, BCVA = best corrected visual acuity recorded in logMAR units; CS = contrast sensitivity, MS = mean sensitivity.  $V_{Total}$  and  $V_{30}$  are volumetric metrics that characterize the total amount of sensitivity in the hill-of-vision as defined by the entire test grid ( $V_{Total}$ ) or that contained within a central circle of 30° radius ( $V_{30}$ ).





ACCEPTED MANUSCRIPT



ACCEPTED MANUSCRIPT

